

2000

Broadening, shifting, and line asymmetries in the $2\leftarrow 0$ band of CO and CO–N₂: Experimental results and theoretical calculations

Adriana Predoi-Cross

J. P. Bouanich

D. Chris Benner

William & Mary, dcbenn@wm.edu

A. D. May

J. R. Drummond

Follow this and additional works at: <https://scholarworks.wm.edu/aspubs>

 Part of the [Biological and Chemical Physics Commons](#)

Recommended Citation

Predoi-Cross, Adriana; Bouanich, J. P.; Benner, D. Chris; May, A. D.; and Drummond, J. R., Broadening, shifting, and line asymmetries in the $2\leftarrow 0$ band of CO and CO–N₂: Experimental results and theoretical calculations (2000). *The Journal of Chemical Physics*, 113, 158-168.
<https://doi.org/10.1063/1.481783>

This Article is brought to you for free and open access by the Arts and Sciences at W&M ScholarWorks. It has been accepted for inclusion in Arts & Sciences Articles by an authorized administrator of W&M ScholarWorks. For more information, please contact scholarworks@wm.edu.

Broadening, shifting, and line asymmetries in the 2←0 band of CO and CO-N₂: Experimental results and theoretical calculations

Cite as: J. Chem. Phys. **113**, 158 (2000); <https://doi.org/10.1063/1.481783>

Submitted: 13 March 2000 . Accepted: 05 April 2000 . Published Online: 21 June 2000

Adriana Predoi-Cross, J. P. Bouanich, D. Chris Benner, A. D. May, and J. R. Drummond



View Online



Export Citation

ARTICLES YOU MAY BE INTERESTED IN

[Shifting and broadening in the fundamental band of CO highly diluted in He and Ar: A comparison with theory](#)

The Journal of Chemical Physics **115**, 2198 (2001); <https://doi.org/10.1063/1.1383049>

[Speed dependence of rotational relaxation induced by foreign gas collisions: Studies on CH₃F by millimeter wave coherent transients](#)

The Journal of Chemical Physics **101**, 6475 (1994); <https://doi.org/10.1063/1.468342>

[Absolute molecular transition frequencies measured by three cavity-enhanced spectroscopy techniques](#)

The Journal of Chemical Physics **144**, 214202 (2016); <https://doi.org/10.1063/1.4952651>

The Journal
of Chemical Physics

Submit Today

The Emerging Investigators Special Collection and Awards
Recognizing the excellent work of early career researchers!



Broadening, shifting, and line asymmetries in the $2\leftarrow 0$ band of CO and CO–N₂: Experimental results and theoretical calculations

Adriana Predoi-Cross^{a)}

Department of Physics, University of Toronto, Toronto, Canada M5S 1A7

J. P. Bouanich

Laboratoire de Photophysique Moléculaire CNRS, Université Paris-Sud, Bâtiment 350, F-91405 Orsay cedex, France

D. Chris Benner

Department of Physics, College of William and Mary, Williamsburg, Virginia 23187-8795

A. D. May^{b)} and J. R. Drummond

Department of Physics, University of Toronto, Toronto, Canada M5S 1A7

(Received 13 March 2000; accepted 5 April 2000)

We have measured the room temperature, widths, pressure shifts, and line asymmetry coefficients for many transitions of the first overtone band of CO and CO perturbed by N₂. The broadening coefficients were obtained with an accuracy of about 1%. The pure CO profiles have been fitted by a Voigt profile while the CO–N₂ spectral profiles have been fitted with a Lorentz and an empirical line shape model (HC_v) that blends together a hard collision model and a speed-dependent Lorentz profile. In addition to the Voigt, Lorentz, and HC_v models, we have added a dispersion profile to account for weak line mixing. The line broadening and shift coefficients are compared to semiclassical calculations employing a variety of intermolecular interactions. The line asymmetry results are compared to line mixing calculations based on the energy corrected sudden (ECS) model. The results indicate that effects other than line mixing also contribute to the measured line asymmetry. © 2000 American Institute of Physics. [S0021-9606(00)01425-2]

INTRODUCTION

In this work we present room temperature, experimental measurements of the broadening, shifting, and line asymmetries in CO and CO–N₂ mixtures for the first overtone band. These spectroscopic parameters are needed for the MOPITT satellite project. The purpose of MOPITT is to measure the concentrations of CO and CH₄ in the troposphere. Specifically for CO, the objective is to obtain profiles with a resolution of 22 km horizontally, 3 km vertically, with an accuracy of 10%. The results of the MOPITT project will be global maps of carbon monoxide and column methane distribution in the troposphere and will lead, through three-dimensional (3D)-modeling, to an increased knowledge of tropospheric chemistry.

In the last 40 years, there have been few laboratory measurements of the broadening^{1–6} and shifting^{3,6} of the first overtone, *P* and *R* branch lines of pure CO or perturbed by N₂. Plyler and Thibault⁷ have summarized the very early measurements of self-broadening. There have been no previous measurements of line asymmetries for the $2\leftarrow 0$ band. This paper reports on the first in a series of high resolution studies planned to extend the range and precision of measurements of the widths and shifts and to measure the weak asymmetry coefficients. One of the results will be to show

that the asymmetries are not entirely due to line mixing.

Models for atmospheric absorption require line parameters over a wide range of pressures and temperatures. To interpolate between experimental values and to extrapolate beyond them, it is essential to support any empirical law by theoretical calculations that establish an understanding of the underlying physics that controls the important line parameters. For this reason we have performed theoretical calculations of the width and shift coefficients using the Robert and Bonamy (RB) formalism⁸ and several interaction potentials. Line mixing coefficients were calculated using the energy corrected sudden (ECS) approximation.^{9,10}

EXPERIMENTAL DETAILS AND RESULTS

The spectra analyzed in this work were recorded using a Bomem DA8.003 Fourier transform spectrometer. The CO spectra were recorded at 0.01 cm⁻¹ resolution using a 1.5 mm aperture. We have used two different cells. The CO–N₂ spectra were recorded using a cell of length 25.06 cm while the pure CO spectra were recorded using a 2.5 cm cell. Both cells were equipped with CaF₂ windows. In order to enhance the signal-to-noise ratio, the InSb detector was provided with a cold, narrow-band filter. The CO–N₂ measurements were made at 303 K at pressures ranging from one to six atmospheres. The pure CO spectra were recorded at room temperature (296 K) over a range of pressures from 30 to 80 torr. For the CO–N₂ measurements a mixture of 5% CO in N₂ was used. The temperature was monitored and stabilized us-

^{a)}Present address: JDS Uniphase Corporation, 570 West Hunt Club Rd., Nepean, Canada K2G 5W8.

^{b)}Author to whom correspondence should be addressed; electronic mail: dmay@physics.utoronto.ca

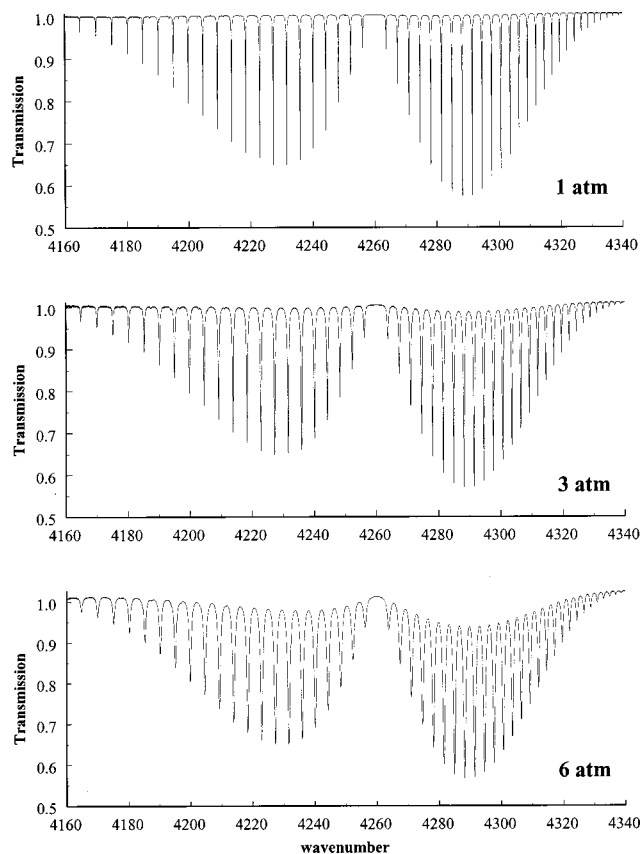


FIG. 1. Sample Fourier-transform infrared spectra of the first overtone of CO at 303 K, perturbed by N₂.

ing an Omega temperature controller. The wave number scale was calibrated using the residual water lines¹¹ produced by absorption within the evacuated spectrometer. The mean uncertainty in frequency for unblended lines is estimated to be ± 0.0005 cm⁻¹. Signal-to-noise ratios in excess of 2000 were achieved for a 1 sec integration time.

As an example, Fig. 1 shows a plot of the transmission spectrum for the first overtone band of CO–N₂ at three different pressures. At one atmosphere the *P* and *R* branch lines are well resolved and there is negligible overlap of adjacent lines. At 3 atm the valley between the lines is just beginning to “fill in.” Prior to an analysis of the profiles, we labeled this the regime of weak line mixing. In hindsight it is the regime of weak asymmetry. At 3 atm, “line mixing” is more severe but there is little or no evidence of the overall collapse of the band that occurs at very high pressures.¹⁰ For CO at the highest pressure (80 torr), the spectrum looks very similar to the 1 atm spectrum presented in this figure for CO–N₂, i.e., there is no overlap between adjacent lines.

We have fitted the experimental absorption coefficients using several line shape models and two computer codes. The CO–CO measurements were made at low pressures, where the Voigt profile convolved with the instrumental line shape function is the appropriate line shape for isolated lines. To this profile we have added the corresponding dispersive term with the original intention of accounting for line mixing. Below we will see that the line asymmetry, *Y*, as defined by the amplitude of the dispersive relevant to the amplitude

of the symmetric (Lorentzian) component of the profile, cannot be ascribed solely to line mixing. For this reason, when discussing the experimental results we will simply refer to asymmetry coefficients. The code¹² for the Voigt profile fits spectra in a 10 cm⁻¹ band at all pressures simultaneously. In essence this forces the width, shifting, and asymmetry to scale linearly with density. In addition to successfully fitting the spectral profiles, the code also models correctly the zero-level, phase error, and parameters associated with the level and shape of the instrumental continuum. The output from the fitting routine are values of the broadening, shift, and asymmetry coefficients. The gas behaves as an almost ideal gas at these low pressures and it is therefore meaningful to follow a practice common in atmospheric work and quote all coefficients in atm⁻¹.

The spectra used to determine the N₂-spectral parameters were all recorded at pressures above one atmosphere. At such pressures the Voigt profile is inappropriate from a physical point of view. For this reason we have chosen to fit our N₂-broadened spectra using a Lorentzian profile with an associated dispersion profile to account for line mixing effects. This program does not incorporate the instrumental line shape. At the pressures used in our study the half-width of the pressure broadened spectral lines was at least ten times larger than the half-width of the instrumental line shape.

A second profile, the speed-dependent hard collision introduced by Henry *et al.*¹³ (called H* in Ref. 13 and labeled HC_v here), was also used to analyze the CO–N₂ data. This profile provides a realistic scaling with density all the way from the low-density Voigt limit to the high-density Dicke narrowing regime.¹⁴ HC_v is distinct from the speed-dependent hard collision model of Rautian and Sobelman.¹⁵ The underlying profile in HC_v is the speed-dependent Lorentzian, *L_v*, given by, $L_v(\omega) = \int f(v) dv / [\Delta\omega^2 + \Gamma(v)^2]$, where *f(v)* is the normalized Boltzmann distribution for the speed, *v*, of the active molecule, $\Delta\omega$ is the frequency measured from line center, and $\Gamma(v)$ is a speed-dependent width. To incorporate the effects of speed-dependent broadening, the Doppler effect and Dicke narrowing,¹⁶ Henry *et al.*¹³ convolved *L_v*(ω) with the hard collision model for the translational motion [called *T_h*(ω) here and *I*(ω) in Eq. (3.4) of Rautian and Sobelman¹⁵]. Thus HC_v can be written as $HC_v(\omega) = T_h(\omega) * L_v(\omega)$, where * indicates a convolution. For completeness we note, if the width is speed independent, that *L_v*(ω) reduces to the well-known Lorentzian profile, $L(\omega) = 1/[\Delta\omega^2 + \Gamma^2]$. Furthermore, if *G*(ω) is the Gaussian profile associated with Doppler broadening, then the Voigt profile, *V*(ω), may be written as $V(\omega) = G(\omega) * L(\omega)$.

The expression for $\Gamma(v)$ used in the speed-dependent profile, HC_v, is the one of Ward *et al.*¹⁷ This model is characterized by a spectroscopic interaction varying as 1/*r* to the power *N* (where *r* is the separation between the center of mass of the active molecule and the perturber) and by a Boltzmann averaged width, $\Gamma_m = \int f(v) \Gamma(v) dv$. Typically, Γ_m and *N* are fitted parameters. In our case *N* was set equal to 6.¹⁴ For both line profiles (HC_v and *L*) the spectra were fit in sections about 10 cm⁻¹ wide at each pressure. The broadening (γ), shifting (δ), and asymmetry (*Y*) coefficients were

TABLE I. Line broadening, shifting, and asymmetry coefficients in the $2\leftarrow 0$ band of pure CO at 296 K as a function of m .

m	γ		
	Voigt model [10^{-3} cm $^{-1}$ atm $^{-1}$]	$\delta(m)$ [10^{-3} cm $^{-1}$ atm $^{-1}$]	$Y(m)$ [10^{-3} atm $^{-1}$]
-20	53.60(49)	-5.48(55)	3.8(7)
-19	54.10(32)	-5.35(44)	2.8(6)
-18	55.60(38)	-5.50(37)	1.1(4)
-17	57.10(21)	-5.15(31)	2.0(4)
-16	58.20(20)	-5.31(27)	-0.3(5)
-15	59.10(16)	-5.31(25)	-2.0(4)
-14	60.20(13)	-4.95(22)	-1.5(4)
-13	61.60(11)	-4.93(20)	-3.7(4)
-12	62.00(9)	-4.72(19)	0.2(4)
-11	62.90(9)	-4.87(18)	0.1(3)
-10	63.90(8)	-4.77(18)	-1.5(4)
-9	64.80(7)	-4.73(17)	-2.4(4)
-8	65.90(7)	-4.64(17)	-2.2(4)
-7	67.10(7)	-4.55(16)	-2.8(3)
-6	69.00(8)	-4.36(16)	-4.1(4)
-5	71.20(7)	-4.14(16)	-4.6(7)
-4	73.90(9)	-3.63(16)	-5.2(5)
-3	77.60(12)	-3.33(18)	-7.3(5)
-2	81.60(19)	-2.73(21)	-8.7(3)
-1	87.40(43)	-2.50(35)	-9.1(6)
1	87.30(33)	-2.26(32)	8.1(5)
2	81.90(16)	-2.99(20)	4.5(5)
3	77.50(10)	-3.26(16)	3.3(3)
4	73.80(7)	-3.34(14)	0.4(5)
5	71.10(6)	-3.55(14)	-0.2(4)
6	68.60(5)	-3.71(14)	-2.5(4)
7	67.10(5)	-3.83(14)	-2.9(3)
8	65.70(5)	-3.79(13)	-3.3(4)
9	64.70(6)	-3.75(13)	-3.6(4)
10	63.60(5)	-3.90(13)	-3.2(5)
11	62.60(5)	-3.81(13)	-5.2(3)
12	61.60(6)	-4.00(14)	-3.1(6)
13	60.60(6)	-4.11(15)	-4.2(6)
14	59.60(7)	-4.27(16)	-5.9(5)
15	58.50(7)	-4.23(16)	-8.1(6)
16	57.50(16)	-4.44(18)	-5.9(5)
17	56.20(11)	-4.35(19)	-7.2(5)
18	55.70(14)	-4.51(22)	-7.4(4)
19	54.30(17)	-4.65(25)	-8.2(5)
20	53.00(23)	-4.81(30)	-9.1(5)
21	52.00(28)	-4.70(36)	-11.7(6)
22	51.50(34)	-5.38(47)	-11.0(7)
23	50.20(42)	-4.73(58)	-12.3(5)

determined from a plot of the appropriate parameters as a function of pressure. For CO-N₂, small corrections were applied to correct for departures from ideal behavior at the higher pressures. The results for CO-CO and CO-N₂ are given in Tables I and II, respectively. The error limits quoted in the tables are one standard deviation. The CO-N₂ results were corrected for self-broadening and shifting.

For CO-CO, the results are plotted in Fig. 2, along with previous measurements near room temperature. For the broadening coefficients, γ , we see there is general agreement between the various measurements²⁻⁴ at low values of the line number, m . For values of $|m| > 5$ the present results are systematically slightly lower than all of the previous measurements. For the shifts, δ , the most recent measurements of Bouanich and co-workers^{3,6} are in agreement with our more

precise values but our measurements are more extensive. To the best of our knowledge there are no previous direct measurements of the CO-CO (assumed) weak mixing or Rosenkranz¹⁸ coefficients for this band.

The results for CO-N₂ are plotted in Fig. 3 and compared with previous measurements. For the broadening coefficients the earlier measurements of Bouanich and Brodbeck³ are higher than ours in the region of m equal to 7 (only the R branch values are plotted). The results of James and Plyler¹ are systematically lower, while the recent results of Voigt *et al.*⁵ are essentially in agreement with our more precise values. For the shifts, the measurements of Bouanich *et al.*⁶ are in agreement with our more precise and more numerous measurements. Once again, there are no previous measurements of the (assumed) weak mixing coefficients. This completes the summary of the experimental results. In the next section we outline the theories used to analyze the measurements.

THEORETICAL CALCULATIONS

Within the usual semiclassical framework, the collisional half-width, γ , and frequency shift, δ , of an isolated, pressure broadened transition are given by,

$$\gamma + i\delta = \frac{n}{2\pi c} \sum_J \rho_J \int_0^\infty u f(u) du \int_0^\infty 2\pi b db S(b, u, J), \quad (1)$$

where n is the number density of the perturber gas, $f(u)$ is the Maxwellian distribution in the relative speed, u , of the absorber-perturber collision pair, ρ_J is the relative population of the perturber in the $|J, v=0\rangle$ state, S is the complex differential cross section representing the collisional efficiency, and b is the impact parameter. Of course Eq. (1) is not correct if speed dependence of the active molecule is important. We ignore this subtlety here. Furthermore, performing the calculations only at the mean relative velocity $\langle u \rangle$ leads to small errors, an insignificant price to pay for a large reduction in computer time.¹⁹ Performing the two integrations separately allows the first to be replaced by $\langle u \rangle$ and the complex differential cross section to be written as $S(b, \langle u \rangle, J)$ or, in condensed notation, as $S^b(b) + iS^s(b)$. Within the RB formalism,⁸ the differential broadening and shifting cross sections $S^b(b)$ and $S^s(b)$, respectively, are given by,

$$S^b(b) = 1 - \exp[\text{Re } S_2^{\text{aniso}}] \times \cos[\text{Im } S_2^{\text{aniso}} + S_1^{\text{iso}}] \quad (2)$$

and

$$S^s(b) = \exp[\text{Re } S_2^{\text{aniso}}] \times \sin[\text{Im } S_2^{\text{aniso}} + S_1^{\text{iso}}], \quad (3)$$

where $\text{Re}(S_2^{\text{aniso}})$ is derived from the anisotropic part of the potential and represents the real part of the second-order perturbation expansion of $S(b)$ in powers of the interaction. $\text{Im}(S_2^{\text{aniso}})$ is nonzero because of the noncommutative character of the interaction at two different times. S_1^{iso} , a real quantity, is the vibrational phase shift arising from the difference in the isotropic part of the potential, V_{iso} , between the initial and final state of the transition. The trajectory model used in this work includes the influence of V_{iso} [taken as a Lennard-Jones (LJ) potential] in the equation of motion around the

TABLE II. Line broadening, shifting, and asymmetry coefficients in the 2←0 band of CO:N₂ at 303 K as a function of m .

m	γ		$\delta(m)$ [10 ⁻³ cm ⁻¹ atm ⁻¹]	$Y(m)$ [10 ⁻³ atm ⁻¹]
	Lorentz model [10 ⁻³ cm ⁻¹ atm ⁻¹]	HC _v model [10 ⁻³ cm ⁻¹ atm ⁻¹]		
-21	50.11(22)	50.60(25)	-5.08(14)	1.0(7)
-20	51.27(20)	51.52(20)	-5.05(16)	1.0(6)
-19	52.00(14)	52.41(15)	-5.06(12)	0.8(4)
-18	52.62(18)	53.29(16)	-5.16(10)	-0.4(4)
-17	53.55(10)	54.14(11)	-5.11(8)	-1.7(5)
-16	54.34(7)	54.96(8)	-5.05(8)	-0.4(4)
-15	54.92(6)	55.74(7)	-5.11(7)	-1.1(4)
-14	56.07(7)	56.50(8)	-5.10(8)	-2.1(4)
-13	56.66(4)	57.23(4)	-5.00(7)	-2.0(4)
-12	57.67(4)	57.94(5)	-4.89(9)	-1.4(3)
-11	58.34(4)	58.65(4)	-4.69(6)	-2.6(4)
-10	59.11(3)	59.39(4)	-4.69(6)	-2.5(4)
-9	59.70(3)	60.19(3)	-4.58(5)	-2.8(4)
-8	60.43(3)	61.11(4)	-4.49(7)	-3.2(3)
-7	61.49(3)	62.25(3)	-4.17(7)	-3.6(4)
-6	62.98(3)	63.73(3)	-3.98(8)	-4.6(7)
-5	65.07(3)	65.74(3)	-3.80(9)	-6.7(5)
-4	67.69(4)	68.49(5)	-3.56(10)	-7.1(5)
-3	71.11(6)	72.11(5)	-3.36(10)	-8.4(3)
-2	75.08(10)	75.64(11)	-2.82(11)	-10.7(6)
-1	80.03(11)	81.03(10)	-3.16(10)	5.6(5)
1	79.85(9)	81.05(8)	-3.33(9)	4.7(5)
2	75.04(7)	75.61(6)	-3.49(8)	2.7(3)
3	71.16(4)	72.12(5)	-3.68(7)	0.9(5)
4	67.79(5)	68.41(4)	-3.67(8)	-0.6(4)
5	65.15(3)	65.50(4)	-3.70(6)	-1.6(4)
6	63.02(4)	63.38(4)	-3.69(7)	-2.2(3)
7	61.29(3)	61.84(3)	-3.64(9)	-2.8(4)
8	60.66(3)	60.69(3)	-3.69(9)	-3.3(4)
9	59.61(2)	59.79(3)	-3.72(9)	-3.7(5)
10	58.55(3)	59.02(2)	-3.71(19)	-4.3(3)
11	57.96(2)	58.32(2)	-3.76(7)	-5.7(6)
12	57.49(3)	57.63(3)	-3.78(7)	-6.1(6)
13	56.48(3)	56.94(3)	-3.81(10)	-6.6(5)
14	55.48(3)	56.23(3)	-3.91(10)	-6.9(6)
15	54.96(3)	55.48(4)	-3.97(10)	-8.0(5)
16	54.32(4)	54.70(4)	-4.10(10)	-8.4(5)
17	53.62(5)	53.89(5)	-4.29(13)	-9.8(4)
18	52.68(6)	53.04(6)	-4.33(15)	-11.0(5)
19	51.61(7)	52.16(7)	-4.40(17)	-11.8(5)
20	50.77(8)	51.27(8)	-4.59(16)	-13.0(6)
21	49.91(8)	50.36(9)	-4.75(15)	-12.8(6)

distance of closest approach. Note in Eqs. (1)–(3) we have suppressed subscripts indicating the initial and final states of the radiator while in Eqs. (2) and (3) we have also suppressed the quantum state of the perturber. Details of a typical calculation are given in Refs. 20 and 21.

Several forms of the intermolecular potential were used in the RB calculations. The first intermolecular potential, V_1 , consists of the sum of electrostatic interactions, V_c , and the Tipping–Herman²² potential, V_{TH} . The most complete electrostatic potential used includes the dipole (μ), quadrupole (Q), octopole (Ω), and hexadecapole (Φ) electrostatic moments of molecules and can be written in the form,

$$V_c = \sum_{\alpha} \sum_{\beta} V_{\alpha\beta}, \quad (4)$$

where for the active molecule (CO) α runs over μ , Q , Ω , and Φ . In the case of N₂ as the perturber, β is limited to Q and Φ . For CO–CO there are a total of 16 terms.

The V_{TH} potential is represented by a three-term expansion in Legendre polynomials as

$$V_{\text{TH}}(r, \theta) = 4\epsilon \left[\left(\frac{\sigma}{r} \right)^{12} - \left(\frac{\sigma}{r} \right)^6 \right] + 24\epsilon \left(\frac{d}{\sigma} \right) \left[2 \left(\frac{\sigma}{r} \right)^{13} - \left(\frac{\sigma}{r} \right)^7 \right] \\ \times P_1(\cos \theta) + 4\epsilon\gamma \left[\left(\frac{\sigma}{r} \right)^{12} - \left(\frac{\sigma}{r} \right)^6 \right] P_2(\cos \theta), \quad (5)$$

where ϵ and σ are the Lennard-Jones parameters, r the intermolecular distance, θ the angle between the molecular axis of CO and the intermolecular axis, and d is the separation of

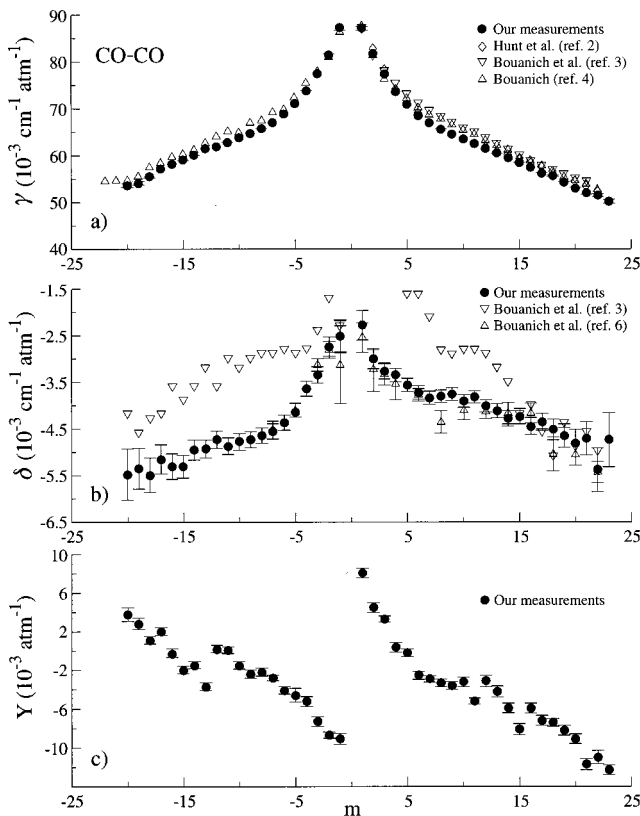


FIG. 2. (a) A comparison of experimental self-broadening coefficients, γ , for the first overtone of CO. (b) A comparison of the self-shifting coefficients, δ , of the first overtone spectrum of CO. (c) Weak mixing coefficients, Y , for the first overtone of CO.

the center of charge from the center of mass of CO. The reduced polarizability anisotropy of CO is defined as $\gamma = (\alpha_{\parallel} - \alpha_{\perp}) / (\alpha_{\parallel} + 2\alpha_{\perp})$. The isotropic part of V_{TH} can be written as,

$$V_{\text{iso}} = \frac{C_{12}}{r_{12}} - \frac{C_6}{r_6} \quad \text{with } C_{12} = 4\epsilon\sigma^{12} \quad \text{and } C_6 = 4\epsilon\sigma^6, \quad (6)$$

where the ϵ and σ are molecule–molecule LJ parameters. Note that the vibrational dependence of the coefficients leads to contributions, ΔC_6 and ΔC_{12} , to S_1^{iso} .

The second potential, V_2 , involves, in addition to the electrostatic potential, an atom–atom potential²³ based on elementary site–site LJ interactions between all the atoms, i , of the active molecule and all the atoms, j , of the perturber and written in the form,

$$V_{ss} = \sum_{i,j} 4\epsilon_{ij} \left[\left(\frac{\sigma_{ij}}{r_{ij}} \right)^{12} - \left(\frac{\sigma_{ij}}{r_{ij}} \right)^6 \right], \quad (7)$$

where the ϵ and σ are atom–atom LJ parameters. The atom–atom potential used in V_2 is obtained from V_{ss} by expressing it as a potential of the form,

$$V_{aa} = \sum_{l_1, l_2, m} U_{l_1, l_2, m}(r) Y_{l_1 m}(\theta_1, \phi_1) Y_{l_2 - m}(\theta_2, \phi_2), \quad (8)$$

where θ_1 , ϕ_1 and θ_2 , ϕ_2 are the orientations of molecules 1 and 2 with respect to the line joining the centers of mass of the two molecules. As in Refs. 8 and 21, the series is trun-

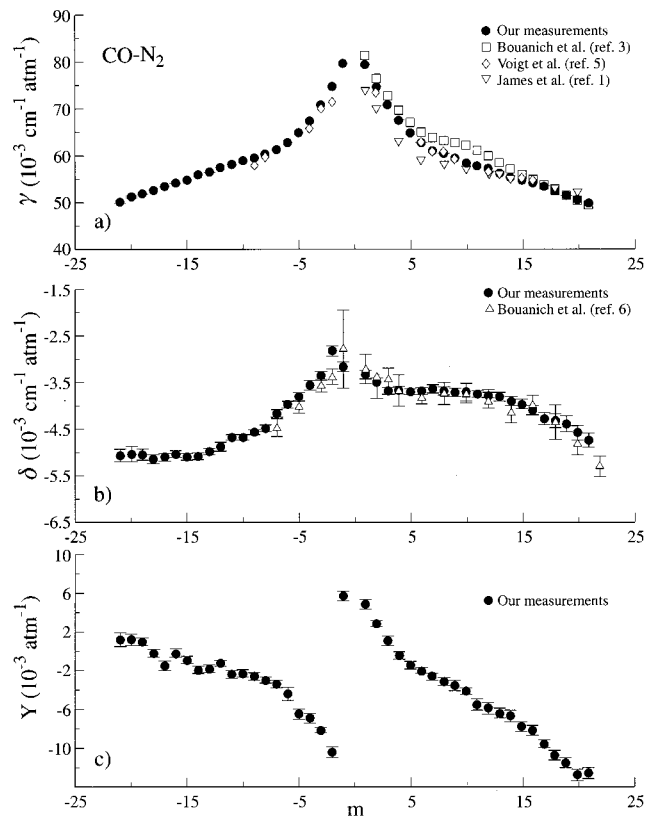


FIG. 3. (a) A comparison of experimental N_2 -broadening coefficients, γ , for the first overtone of CO. (b) A comparison of the N_2 -shifting coefficients, δ , of the first overtone spectrum of CO. (c) N_2 weak mixing coefficients, Y , for the first overtone of CO.

cated at $l_1 + l_2 = 4$. The radial functions are themselves expanded in inverse powers of the separation of the centers of mass, expressed as a sum of LJ potentials. In general, the terms retained are LJ(6,12), LJ(8,14), and LJ(10,16). Below, a further approximation is made for U_{000} .

The values of the potential parameters used in the calculations were all taken from other sources, i.e., they were not adjusted to fit the present experimental results. The molecular, as opposed to the site–site, LJ parameters are needed both to determine the trajectory around the distance of closest approach and in the Tipping–Herman potential. For CO–CO the values were taken from Hirschfelder, Curtis, and Bird.²⁴ The CO– N_2 parameters were obtained using the usual combination rules and the LJ parameters of CO–CO and the revised LJ N_2 – N_2 values from Ref. 25. The value of d , the separation of the CO center of charge and center of mass, was taken from Friedmann,²⁶ while the value of the dimensionless anisotropy of the polarizability was taken from the compilation (Table D.3) of Gray and Gubbins.²⁷ We have used a value of 0.089. The experimental values of 0.1098 D²⁸ and $-2.0 \text{ D}\text{\AA}$,²⁹ were used for the dipole and quadrupole moment of CO. For the higher moments we have used the theoretical values,³⁰ $\Omega = 2.56 \text{ D}\text{\AA}^2$ and $\Phi = -3.40 \text{ D}\text{\AA}^3$, respectively. The odd multipole moments of N_2 are zero. For Q we have used the value of Flygare and Benson³¹ ($-1.40 \text{ D}\text{\AA}$) and for Φ we have used the value of Stone *et al.*³² ($-3.40 \text{ D}\text{\AA}^3$). The numerical values of the atom–atom potential were computed using the site–site LJ param-

eters of Bouanich.³³ Since the code for the trajectory is written in terms of a LJ potential, the isotropic part of the atom–atom interaction, $U_{000}(r)$, was fitted to an LJ(6, n) form, where n is not necessarily an integer. The fitted values of n , σ , and ϵ for CO–CO are 14.6, 3.6529 Å, and 91.104 K, respectively. The corresponding numbers for CO–N₂ are 14.4, 3.6851 Å and 85.361 K. The molecular constants can be taken from Herzberg³⁴ or Reuter *et al.*³⁵ or they may be determined from the Dunning parameters of George *et al.*³⁶ All of the above constants have been determined independently of measurements of the broadening and shifting of the spectral lines.

The isotropic LJ potentials depend upon the CO internuclear separation. It is the difference between the vibrational matrix elements of the potential that leads to the $\Delta C_6/C_6$ and $\Delta C_{12}/C_{12}$ or $\Delta C_n/C_n$ contributions to the shift. These quantities are not known independent of the shifts. They have been fitted from previous measurements of shifts in the fundamental³⁷ and the first overtone⁶ of CO perturbed by CO or N₂. The presently accepted value of $\Delta C_6/C_6$ is 0.009 for the 2←0 band and the ratio $y = (\Delta C_n/C_n)/(\Delta C_6/C_6)$ (for $n = 12$ or $n \sim 14$ –15) is 1.6.

We have also considered two other potentials V'_1 and V'_2 formed by dropping the terms in V_1 and V_2 that involve the octopole and hexadecapole from the electrostatic potential. For CO–CO, V_e contains the weak dipole–dipole and the weak quadrupole–dipole interactions. For both CO–CO and CO–N₂, V_e contains the strong quadrupole–quadrupole interaction and the weak dipole–quadrupole interaction.

Using these potentials the broadening and shifting coefficients for CO–CO at 296 K and CO–N₂ at 303 K were computed by including the contributions from perturbing molecules in the fundamental vibrational state with J values up to 42 for CO and 41 for N₂ each weighted by the Boltzmann factor and the nuclear spin factor (1 for CO and $[(-1)^{J^2} + 3]/2$ for N₂). The results will be presented below.

One drawback to using the RB formalism is that it has not been formulated to account for line mixing, being restricted to the diagonal elements of the relaxation matrix. The ECS formalism does allow us to treat mixing. While it is not cast in terms of the molecular interaction, it has a sound theoretical base. Its strength lies in its ability to model broadening and mixing for an entire absorption spectrum with only a few parameters. Its weakness is that shifting must be inserted “by hand.” This is not a serious drawback as shifting is weak in the present case.

It is well known¹⁸ that the mixing coefficients describing the asymmetric component of weakly overlapping lines are linear functions of the off-diagonal elements of the relaxation matrix. Here we summarize the ECS model for the relaxation matrix. Let i represent the quantum numbers in the initial state and f those in the final state of a transition. Here $i = (j_i, v_i = 0)$ and $f = (j_f, v_f = 2)$. The off-diagonal elements of the relaxation matrix $W(if \leftarrow i'f')$ ³⁸ are related to generalized cross sections, $\sigma(if \leftarrow i'f')$, by,

$$W(if \leftarrow i'f') = \frac{n\langle u \rangle}{2\pi c} \sigma(if \leftarrow i'f'), \quad (9)$$

where, to repeat, n is the number density of perturbers and $\langle u \rangle$ is the mean relative velocity.

In several significant papers, Goldfam *et al.*^{39,40} and Green⁴¹ showed, by starting with the close coupled formalism and making a sudden approximation, that the generalized cross sections, for the interaction of a rigid spherical top molecule and an atomic perturber, may be written in the form,

$$\sigma_{j_i j_f, j'_i j'_f}^{l_i l_f} = \left(\frac{[j'_i]}{[j_i]} \right)^{1/2} \sum_L [L] F_{j_i j_f, j'_i j'_f}^{l_i l_f L} Q_L, \quad (10)$$

where l_i, l_f , the angular momenta along the symmetry axis, are zero for a linear molecule like CO. F , a combination of $3j$ and $6j$ symbols, is a “spectroscopic coefficient” containing the geometry of the interaction with the field and the interaction potential and the Q 's are dynamical factors or effectively reduced cross sections that contain the intrinsic collisional dynamics. Throughout this section, $[x]$ means $(2x+1)$. In an approximate but clever boot-strap calculation, de Pisto *et al.*⁴² removed the sudden restriction from Eq. (10). This introduces adiabaticity factors, Ω . The ECS model invokes the rigid-rotor version of the general result, in which case the Q_L become the rate of population transfer from the rotational state L to the ground rotational state. Temkin *et al.*⁴³ expanded the $6j$ symbols in terms of $3j$ symbols, writing the generalized cross section as

$$\begin{aligned} \sigma_{j_i j_f, j'_i j'_f}^{l_i l_f} &= (-1)^{j_f + j'_f} ([j_f][j'_f])^{1/2} \\ &\times \sum_l \begin{pmatrix} j_i & 1 & j_f \\ l+l_f & -l & -l_f \end{pmatrix} \\ &\times \begin{pmatrix} j'_i & 1 & j'_f \\ l+l_f & -l & -l_f \end{pmatrix} \Gamma_{j_i j'_i}^{l_i l_f + l}, \end{aligned} \quad (11)$$

where the 1 in the $3j$ symbols arises because we are considering dipole absorption. In the case of diatomic molecules, the index, l , can only take on values of 0 and 1. The state-to-state cross sections, Γ , contain the Q_L 's. It is at this level that the adiabaticity factors are introduced and the rates generalized to include the diagonal elements of the relaxation matrix. This leads to the following expression^{9,44} for the basic cross sections,

$$\begin{aligned} \Gamma_{j_i j'_i}^{0l} &= \tau_j^{-1} \delta_{j j'} + \left(\frac{\rho_{j>}}{\rho_j} \right) \Omega_{j>} [j<] (-1)^l \\ &\times \sum_{L \neq 0} [L] \begin{pmatrix} j_i & L & j'_i \\ 0 & 0 & 0 \end{pmatrix} \begin{pmatrix} j_i & L & j'_i \\ l & 0 & -l \end{pmatrix} Q_L \Omega_L^{-1}, \end{aligned} \quad (12)$$

where $j < (j >)$ is the smallest (largest) value of the pair (j_i, j'_i) . The populations, ρ , are introduced in a manner that guarantees detailed balance. The adiabaticity factors, Ω , are given by,

$$\Omega_j = \left(1 + \frac{\Delta \omega_j^2 J_c^2}{24 \langle u \rangle^2} \right)^{-2}, \quad (13)$$

where $\Delta \omega_j$ is the energy spacing between the rotational states ($j >$, $j <$ or L) and the next lower rotational state to

which an inelastic collisional transition may occur. Finally, l_c is a scaling length that is related to the finite duration of a collision.

The basic rates Q_L are given by the gap law

$$Q_L = A(E_L/B)^{-\alpha} \exp(-\beta E_L/kT), \quad (14)$$

where E_L is the rotational energy of level L ($\neq 0$), B the rotational constant, and A , α , and β are constants.

Since Eq. (12) guarantees detailed balance for the off-diagonal elements of the relaxation matrix, the linear relationship between the weak mixing coefficients, Y , and the elements of W becomes,

$$Y_{if} = -2 \sum \frac{d_{i'f'} W(if \leftarrow i'f')}{d_{if}(v_{i'f'} - v_{if})}, \quad (15)$$

where the v 's indicate the transition frequencies and the sum is over the lines ($i' \rightarrow f'$). It is common practice to label the line of interest, ($i \rightarrow f$) by l and the interfering line ($i' \rightarrow f'$) by k . Thus the sum in Eq. (14) is over k , W may be labeled W_{1k} , and the frequency difference written as ($v_k - v_l$). There are a variety of methods of fixing the parameters of the ECS model (A, β, α, l_c). Below, we fix the parameters by fitting the measured broadening coefficients. This does not introduce additional variables (τ_j 's), since they are fixed in terms of the other ECS parameters⁴⁴ by a sum rule [see Eqs. (5), (7), and (8) in Ref. 9].

COMPARISON OF EXPERIMENT AND CALCULATIONS

Broadening coefficients, γ

First we compare the RB calculations of the broadening coefficients with the measured values. Experimentally, the broadening coefficients are symmetric in the line number m . This is consistent with the calculations $\text{Im}(S_2^{\text{aniso}})$ being small. The results for CO–CO, calculated with V_1 and V'_1 , are shown in Fig. 4(a). For V_2 and V'_2 they are shown in Fig. 4(b). The corresponding comparison between calculated and measured broadening coefficients for CO–N₂ are found in Figs. 5(a) and 5(b). All potentials yield results that are in semiquantitative agreement with the measured values. The figures would appear to indicate a preference for the potentials built around the Tipping–Herman potential (V_1 and V'_1) over those built around atom–atom potential (V_2 and V'_2). However, in a recent article,⁴⁵ Bruet *et al.* have shown that RB semiclassical (SC) calculations, for a given potential, yield broadening coefficients that may be in error by some 10% when compared with coupled state (CS) calculations. The latter are themselves known to reproduce the full close coupled (CC) calculations within about 1%. There are two aspects to this theoretical disagreement. One has to do with the validity of a semiclassical theory itself and the second with the fact that the RB formalism does not give an exact solution to the semiclassical problem. For heavy particles the second difficulty is probably the most serious. Nevertheless, without performing a coupled state calculation or an exact semiclassical calculation (with our potentials) it is not possible to separate the contribution to the widths of (i) errors in the potentials from (ii) the bias in the RB calculations. This is not a serious problem for atmospheric work. The complex-

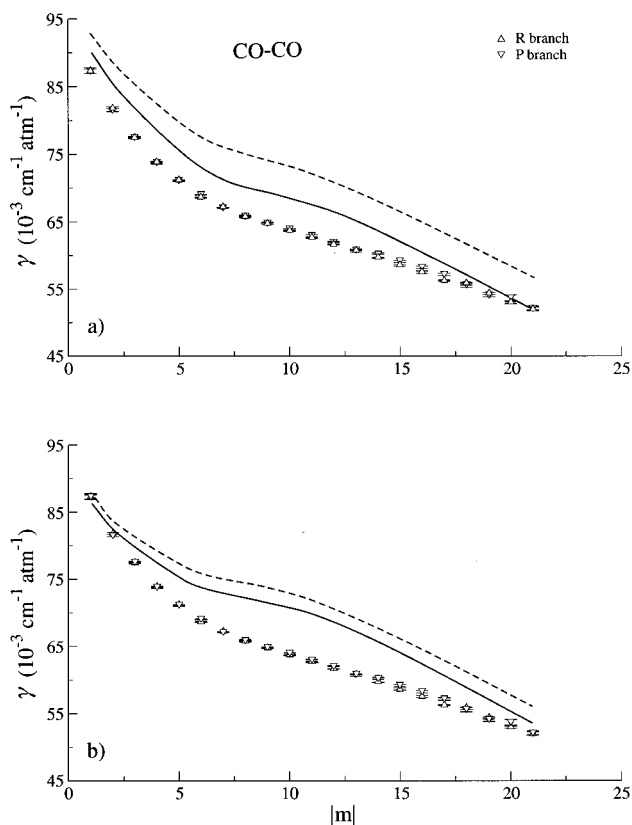


FIG. 4. CO–CO broadening coefficients for CO lines in the 2–0 band at 296 K. The triangles with error bars represent the experimental values obtained in this work. The curves in (a) represent the calculated results derived from the potentials involving the Tipping–Herman potential, those in (b) involve the atom–atom potential. Dashed curves for V_1 or V_2 , solid lines for V'_1 or V'_2 .

ity of modeling atmospheric absorption precludes any theoretical calculations of the broadening and shifting. These parameters are always measured but never over the complete range of variables encountered in the atmosphere. The main advantage of the RB formalism for atmospheric work comes from the fact that it gives broadening coefficients that are semiquantitative (provided we have a reasonable potential) and it is easy to implement. Therefore it can be used to establish scaling rules that permit one to extrapolate experimental results to other regions of parameter space (pressure, temperature, composition). A prime example of a temperature scaling rule is that of Bonamy *et al.*⁴⁶

We note, for a given potential, that the level of discrepancy is not the same for CO–CO as for CO–N₂. Since the dominant source of the broadening is the quadrupolar interaction, we are led to suspect that the relative value of the quadrupole moment for CO and N₂, that we have used is in error. An absolute value for the quadrupole of CO less than or equal to 1.8 DÅ, accompanied by an absolute value for the quadrupole moment of N₂ larger or equal to 1.5 DÅ, will bring the calculated broadening coefficients for CO–CO and CO–N₂ to the same satisfactory level of agreement with the experimental values. Such values for the quadrupole moment of CO lie outside of the range of values recently reported in the literature.²⁷

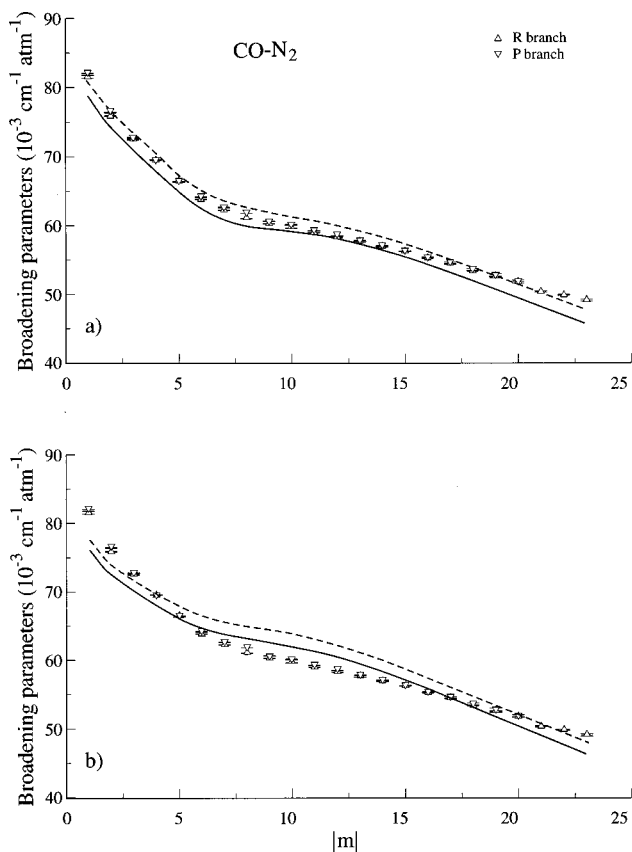


FIG. 5. CO–N₂ broadening coefficients for CO lines in the 2←0 band at 303 K. The triangles with error bars represent the experimental values obtained in this work. The curves in (a) represent the calculated results derived from the potentials involving the Tipping–Herman potential, those in (b) involve the atom–atom potential. Dashed curves for V_1 or V_2 , solid lines for V_1' or V_2' .

Shifting coefficients, γ

Calculations show that the shifts are insensitive to inclusion of the higher order anisotropic electrostatic interactions. Therefore we compare the measured shifts with those calculated using V_1' and V_2' . As shown earlier,⁴⁷ there is an advantage in comparing the parts of the shifts symmetric and antisymmetric in m rather than the total shifts. The reason for this can be found in the RB formalism. In Eq. (3), S_1^{iso} is symmetric and $\text{Im}(S_2^{\text{aniso}})$ is antisymmetric in the line number, m . Furthermore, if the exponential and the sine are expanded then there is a first-order term, S_1^{iso} , that contributes to the shift. The latter varies directly with ΔC_6 and ΔC_{12} or ΔC_n . The terms in S_2^{aniso} are independent of the C 's, depending only on the anisotropic part of the potential. Experimental values of the symmetric and asymmetric components of the shifts (for each value of the line number, m) are readily constructed from $\delta_s(m) = [\delta(m) + \delta(-m)]/2$ and $\delta_a(m) = [\delta(m) - \delta(-m)]/2$, respectively.

Figures 6(a) and 6(b) show a comparison of the experimental and calculated symmetric components of the shift. Overall, for both CO–CO and CO–N₂, the calculated values of δ_s are in semiquantitative agreement with the measured values. For CO–N₂, the symmetric part of the shift calculated with V_1' is in excellent agreement with the experimental values. Above, we indicated for the broadening that one does

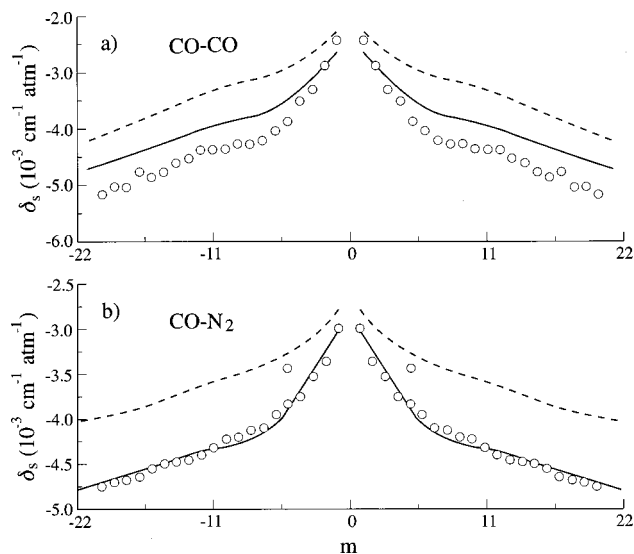


FIG. 6. Symmetric components (δ_s) of the line shifts for (a) CO–CO and (b) CO–N₂ in the 2←0 band at 296 K. The circles were derived from the experimental data of the line shifts. The curves represent the theoretical results derived from the potentials in which the electric multipole moments higher than the quadrupole were omitted. Solid curve for V_1' , dashed curve for V_2' .

not expect the SC theory of RB to yield the exact CC results. It is probably safe to say, for the present systems, that the main problem lies not in the fact that the RB theory is semiclassical, but rather in the fact that it is an approximate solution to the full SC theory. It fails, as do most other SC calculations, to respect the lack of commutivity of the interaction at different times to all orders of the interaction. The question of commutivity only arises at the second or higher order. Thus we expect the mean shift (shift of the overtone vibrational frequency) to be well determined in the RB calculation since it is small and arises from the first-order term S_1 . Of course, we mean it will be well determined provided the vibrational dependence of the isotropic component of the potential is well known. We could then legitimately vary ΔC_6 and ΔC_{12} to move the calculated values of δ_s , up or down overall, in order to bring the calculated component of the symmetric part of the shift into closer agreement with the measured values. This we do not do since the two contributions to the shift of the vibrational frequency have opposite signs and a different temperature dependence, and thus a better approach to determining the vibrational dependence would be to fit measurements over a wide range of temperature.

The variation of δ_s with line number that is apparent in Figs. 6(a) and 6(b), arises from the real part of S_2^{aniso} . The potential appears to lead to a variation with m that is closer to the experimental results. This is surprising, given that one of the main reasons for introducing an atom–atom description of the interaction was to improve the short-range anisotropic potential. The question of lack of commutivity does not arise in determining the real part of S_2^{aniso} .

Now consider that part of the shift that is antisymmetric in line number. In the RB form of the SC theory, δ_a is nonzero because the imaginary part of S_2^{aniso} is nonzero. The

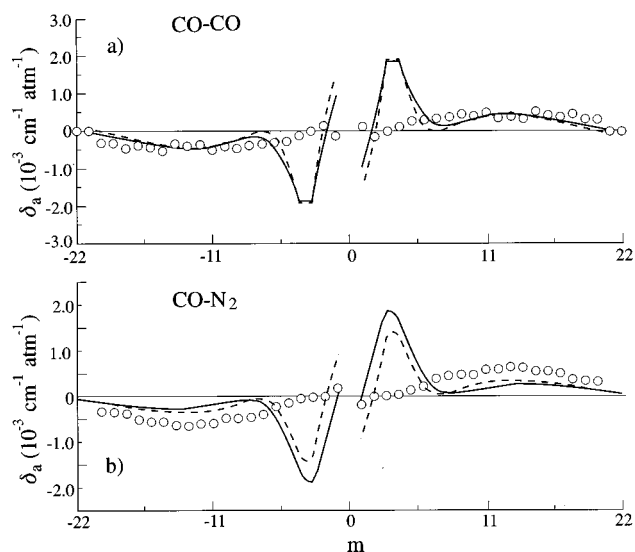


FIG. 7. Antisymmetric components (δ_a) of the line shifts for (a) CO–CO and (b) CO–N₂ in the 2←0 band at 303 K. The circles were derived from the experimental data of the line shifts. The curves represent the theoretical results derived from the potentials in which electric multipole moments higher than the quadrupole are omitted. Solid curve for V_1' , dashed curve for V_2' .

experimental and calculated values of the shift antisymmetric in m are shown in Figs. 7(a) and 7(b) for CO–CO and CO–N₂, respectively. Here we see that the experimental and calculated values differ qualitatively. In Ref. 47 the discrepancy is ascribed to the fact that the RB formalism does not go to high enough order, while still accounting for the lack of commutivity. It is known that the approximate (commutivity assumed) but infinite order theory of Smith *et al.*⁴⁸ can lead to a significant value of δ_a .⁴⁹ However, in some unpublished work on CO–Ar we have shown that the theory of Smith *et al.* is not sufficient, alone, to explain the qualitative features of Figs. 7(a) and 7(b). This indicates the semiclassical theory must be kept exact to orders higher than the second.

Asymmetry coefficients, γ

As pointed out above, the RB formalism has not been extended to include line mixing. On the other hand, the ECS model captures line broadening and mixing and is well suited to modeling atmospheric absorption. Within the ECS model, line shifting must be inserted “by hand.” In order to compare ECS calculations of weak mixing coefficients and our asymmetry coefficients, we need the ECS parameters. To determine the parameters, we can either determine them from fitting high pressure, strong mixing profiles from other experiments or we can fix the parameters using the present broadening coefficients. For CO–CO, the ECS parameters, A , α , β , and l_c , as determined from both methods, are 8.695 (10.94) $10^{-3} \text{ cm}^{-1} \text{ atm}^{-1}$, 3.924 50 (2.7384), 0.000 (0.1816), and 0.180 (0.240) Å, respectively, where the quantities in brackets refer to values obtained from spectra at high pressures.¹⁰ The unbracketed results were determined from the present measured broadening coefficients. The corresponding values for CO–N₂ are 8.751 (4.117)

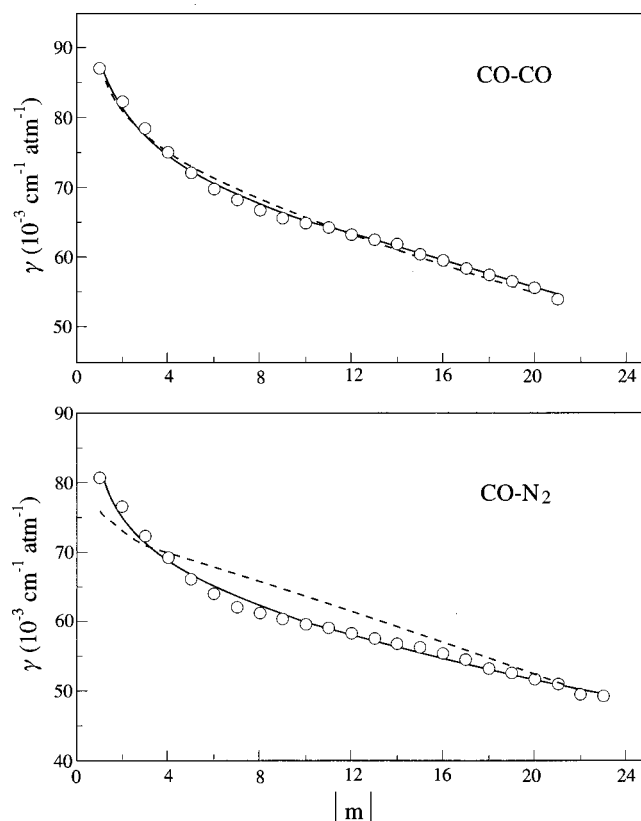


FIG. 8. A comparison of experimental broadening coefficients (circles) and values fitted to the ECS model (solid line). The dashed line shows the broadening coefficients as calculated using ECS parameters derived from fitting high pressure band profiles.

$10^{-3} \text{ cm}^{-1} \text{ atm}^{-1}$, 4.409 (1.7889), 0.000 (0.0046) and 0.153 (0.330) Å. Actually, the parameters in brackets for CO–N₂ are values derived from fitting calculated broadening coefficients which, as previously shown,¹⁰ leads to spectra that reproduce the experimental curves at high pressures. We can thus consider them to being equivalent to values derived from fitting directly the curves at high pressure. We see that the two sets of ECS parameters are much closer for CO–CO than for CO–N₂. In all cases, we have followed Bouanich *et al.*¹⁰ and taken the nearest state to which an inelastic transition may occur to differ in rotational quantum number by 2.

As might have been noted earlier, there is little difference between the broadening measured in the P and R branch. Near equality of the two is built into the ECS model. In Fig. 8, we show by a solid line the ECS fitted values, along with the average of the measured values of the P and R branch, as a function of the absolute value of the line number, m . The fit is reasonable for both CO–CO and CO–N₂. On the other hand, the value of the broadening coefficients as predicted using ECS parameters determined from high pressure data¹⁰ is relatively poor for the case of CO–N₂. It has already been implied¹⁰ that it is not possible in this case to find ECS parameters that describe equally well both broadening coefficients and spectra in the strong mixing limit.

In Fig. 9 we compare the measured asymmetry coefficients with the line mixing coefficients calculated using the ECS parameters as determined from the broadening (solid

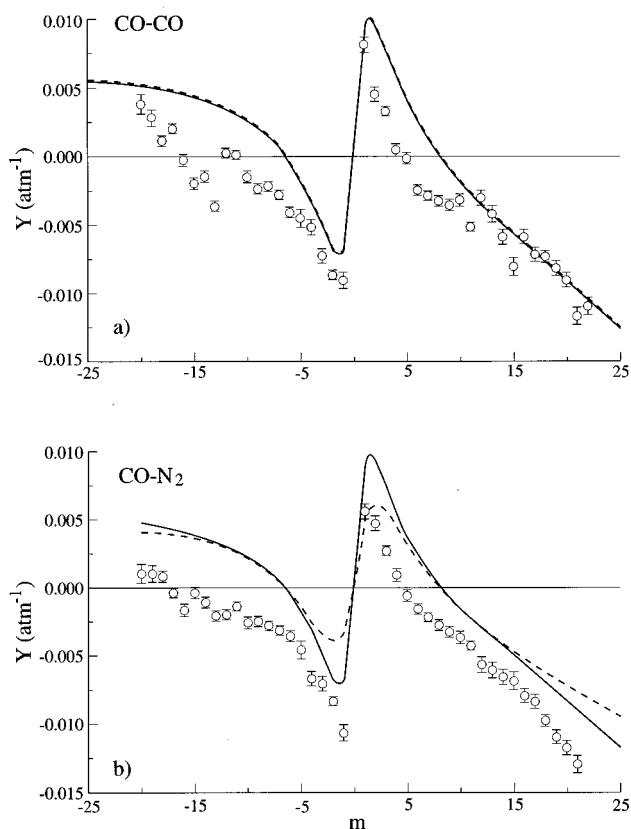


FIG. 9. A comparison of experimental weak mixing coefficients (circles) and values calculated using ECS parameters derived from fitting the broadening coefficients (solid line) or calculated using ECS parameters derived from fitting high pressure band profiles (dashed line).

line) and as determined using the profiles in the strong mixing limit (dashed line). Consider first the calculated values. In the case of CO–CO the two calculated values are in close agreement. Perhaps surprising is the fact that the two calculated curves are relatively close also for CO–N₂, with a measurable difference occurring only at very low and very high values of m . Given that the calculated mixing parameters appear to be relatively insensitive to the values of the ECS parameters, it is safe to conclude that the calculated mixing coefficients should be close to the experimental values, provided the asymmetries arise purely from line mixing. However, the measured asymmetries are only qualitatively in agreement with the calculated values. The disagreement between the calculated and the measured values of the asymmetry parameters is well outside the experimental (random) error as reported by the fitting routine. We conclude that the measured asymmetries arise only in part from line mixing.

Besides the quantitative disagreement between the measured asymmetries and the calculated line mixing coefficient, there are other signs that the measured asymmetries are not to be ascribed solely to line mixing. If we ignore speed-dependent effects then we expect line mixing to be primarily within a branch, with interbranch (P and R) mixing appearing only at low values of line number [see the dependence on frequency separation in Eq. (14)]. With or without interbranch mixing we expect the mixing in the two branches to be almost the same in magnitude but opposite in sign (the

lines are approximately equally spaced but the frequency factors are reversed between the P and R branch). Neither of these expectations is realized for the experimental values. If $S(m)$ is the line strength then the sum rule,⁵⁰ $\sum S(m)Y(m) = 0$, requires the mixing coefficients to pass through zero near or at the center of gravity of a branch, i.e., near $|m| = 7$. The experimental values do not exhibit this property. In fact, numerically, the sum rule is strongly violated by the measured asymmetries. It seems inescapable to reach the conclusion that the measured asymmetries arise both from line mixing and other sources of line asymmetries. On the positive side, the results indicate that it may be possible to use the ECS model to estimate the line mixing asymmetry and remove it from the measured quantity, thus isolating the other contributions to line asymmetries.

One other source of asymmetries is the speed dependence of the relaxation. The reason for fitting the profiles with HC_v was to allow for speed-dependent broadening which is known to exist, both from the present experiment and previous experiments.¹⁴ What is not ruled out is the possibility of having a speed-dependent broadening (without an asymmetry) for an isolated line and to have additional asymmetric speed-dependent effects in line mixing. As pointed out by May,³⁸ the various relaxation rates appearing in the master dynamical equation for the off-diagonal elements of the density matrix may be classified as optical coherence changing, velocity changing, and a combination of both. He labeled the latter as type III and these are the source of statistical correlation between the relaxation of the components of the optical coherence and the velocity components. Being off-diagonal in the component of the optical coherence (line), we can then reason that the effects of statistical correlation will appear in line mixing and grow with pressure.

It is well known that the finite duration of collision also produces line asymmetries that grow with density.⁵¹ In a recent article, Boissoles *et al.*⁵² discussed asymmetries in HF–Ar that may arise from speed-dependent shifting and the finite duration of collision. Intuitively one expects the effects of the finite duration of collision to be line independent and thus to shift all of the measured asymmetries in one direction. There is some evidence for this in the present experiment since all of the measured asymmetry parameters are lower than those calculated using an ECS model for line mixing. Clearly there are several sources of line asymmetries in CO, self-perturbed or perturbed by N₂. Unraveling the different contributions will require a full calculation of the profile with a well-established potential. Since the intrinsic dynamical equation³⁸ is even more complicated than the well-known Boltzmann equation, it can only be solved numerically. However, a prudent “first step” would be an independent measurement of the mixing coefficients in this overtone band. The results reported here are at variance with those reported earlier for the fundamental band.⁵³

CONCLUSION

We have measured the line broadening, shifting, and asymmetry coefficients in pure CO and in CO–N₂, both near room temperature. These parameters are required for remote sensing of the atmosphere and as such must be known over a

range of pressures and temperature. We have shown that the broadening and the major part of the shifting are in qualitative agreement with the semiclassical calculations of Robert and Bonamy. Thus the theory may be used to establish scaling rules for these parameters. The shifts, asymmetric in line number, are in qualitative disagreement with the RB formalism as were the ECS calculations of weak mixing coefficients. In all cases the sources or possible sources of the discrepancies between the measured and calculated coefficients were discussed. In particular, it is argued that the line asymmetries are not due to line mixing alone.

ACKNOWLEDGMENTS

This work was supported by funding from the Natural Sciences and Engineering Research Council of Canada, COMDEV, BOMEM Inc., the Meteorological Service of Canada, the University of Toronto Research Fund, and the Canadian Space Agency. We are grateful to R. Berman for several fitting routines and numerous discussions.

- ¹T. C. James and E. K. Plyler, *J. Chem. Phys.* **40**, 221 (1964).
- ²R. H. Hunt, R. A. Toth, and E. K. Plyler, *J. Chem. Phys.* **49**, 3909 (1968).
- ³J. P. Bouanich and C. Brodbeck, *J. Quant. Spectrosc. Radiat. Transf.* **13**, 1 (1973). This reference contains graphs of the shift for CO–N₂ which are difficult to duplicate for a comparison with the present measurements.
- ⁴J. P. Bouanich, *J. Quant. Spectrosc. Radiat. Transf.* **31**, 561 (1984).
- ⁵S. Voigt, S. Dreher, J. Orphal, and J. P. Burrows, *J. Mol. Spectrosc.* **180**, 359 (1996).
- ⁶J. P. Bouanich, D. Bermejo, J. L. Domenech, R. Z. Martinez, and J. Santos, *J. Mol. Spectrosc.* **179**, 22 (1996).
- ⁷E. K. Plyler and R. J. Thibault, *J. Res. Natl. Bur. Stand., Sect. A* **67**, 229 (1963).
- ⁸D. Robert and J. Bonamy, *J. Phys. (Paris)* **40**, 923 (1979).
- ⁹L. Bonamy, J. Bonamy, S. Temkin, D. Robert, and J. M. Hartmann, *J. Chem. Phys.* **98**, 3747 (1993).
- ¹⁰J. P. Bouanich, R. Rodrigues, and C. Boulet, *J. Quant. Spectrosc. Radiat. Transf.* **54**, 683 (1995).
- ¹¹R. A. Toth, *J. Opt. Soc. Am. B* **8**, 2236 (1991).
- ¹²D. C. Benner, C. P. Rinsland, V. Malathy Devi, M. A. H. Smith, and D. Atkins, *J. Quant. Spectrosc. Radiat. Transf.* **53**, 705 (1995).
- ¹³A. Henry, D. Hurtmans, M. Margottin-Maclou, and A. Valentin, *J. Quant. Spectrosc. Radiat. Transf.* **56**, 647 (1996).
- ¹⁴R. Berman, P. M. Sinclair, A. D. May, and J. R. Drummond, *J. Mol. Spectrosc.* **198**, 283 (1999).
- ¹⁵S. G. Rautian and I. I. Sobelman, *Sov. Phys. Usp.* **9**, 701 (1967).
- ¹⁶R. H. Dicke, *Phys. Rev.* **89**, 472 (1953).
- ¹⁷J. Ward, J. Cooper, and E. Smith, *J. Quant. Spectrosc. Radiat. Transf.* **14**, 555 (1974).
- ¹⁸P. W. Rosenkranz, *IEEE Trans. Antennas Propag.* **AP-23**, 498 (1975).
- ¹⁹J. P. Bouanich, G. Blanquet, and J. Walrand, *J. Quant. Spectrosc. Radiat. Transf.* **42**, 319 (1989).
- ²⁰J. P. Bouanich and G. Blanquet, *J. Quant. Spectrosc. Radiat. Transf.* **40**, 205 (1988).
- ²¹J. P. Bouanich, D. Lambot, G. Blanquet, and J. Walrand, *J. Mol. Spectrosc.* **140**, 195 (1990).
- ²²R. H. Tipping and R. M. Herman, *J. Quant. Spectrosc. Radiat. Transf.* **10**, 881 (1970).
- ²³J. Bonamy and D. Robert, *J. Quant. Spectrosc. Radiat. Transf.* **16**, 185 (1976).
- ²⁴J. O. Hirschfelder, C. F. Curtiss, and R. B. Bird, *Molecular Theory of Gases and Liquids* (Wiley, New York, 1967).
- ²⁵J. P. Bouanich, G. Blanquet, and J. Walrand, *J. Mol. Spectrosc.* **161**, 416 (1993).
- ²⁶H. Friedmann, *Adv. Chem. Phys.* **4**, 225 (1962).
- ²⁷C. G. Gray and K. E. Gubbins, *Theory of Molecular Fluids* (Oxford University Press, New York, 1984).
- ²⁸J. S. Muentzer, *J. Mol. Spectrosc.* **55**, 490 (1975).
- ²⁹F. E. Budenholzer, E. A. Gislason, A. D. Jorgensen, and J. G. Sachs, *Chem. Phys. Lett.* **47**, 429 (1977).
- ³⁰G. Maroulis, *Z. Naturforsch. A: Phys. Sci.* **47**, 480 (1991).
- ³¹W. H. Flygare and R. C. Benson, *Mol. Phys.* **20**, 225 (1971).
- ³²N. W. B. Stone, L. A. A. Read, A. Anderson, I. R. Dagg, and W. Smith, *Can. J. Phys.* **62**, 338 (1984).
- ³³J. P. Bouanich, *J. Quant. Spectrosc. Radiat. Transf.* **4**, 243 (1992).
- ³⁴G. Herzberg, *Spectra of Diatomic Molecules* (Van Nostrand, New York, 1950).
- ³⁵D. Reuter, D. E. Jennings, and J. W. Brault, *J. Mol. Spectrosc.* **115**, 294 (1986).
- ³⁶T. George, W. Urban, and A. Le Floch, *J. Mol. Spectrosc.* **165**, 500 (1994).
- ³⁷J. P. Bouanich, F. Rachet, and A. Valentin, *J. Mol. Spectrosc.* **178**, 157 (1996).
- ³⁸A. D. May, *Phys. Rev. A* **59**, 3495 (1999). As discussed in this reference, the relaxation matrix $W(if \leftarrow i'f')$ describes the transfer by collision from the $i'f'$ component of the density matrix (an optical coherence) to the if component of the density matrix. The usual nomenclature of line space involves labeling the transitions by l and m , say, and writing an element of the relaxation matrix as $W_{l,m}$. Retaining the full tetradic nomenclature helps to prevent confusion between these transfer rates and rates of population transfer. (Populations are a diagonal element of the density matrix and the transfer rates are dyadics.) It is a common practice to make a random phase approximation, in which case the tetradic elements of W become dyadics.
- ³⁹R. Goldflam, S. Green, and D. J. Kouri, *J. Chem. Phys.* **67**, 4149 (1977).
- ⁴⁰R. Goldflam, D. Kouri, and S. Green, *J. Chem. Phys.* **67**, 5661 (1977).
- ⁴¹S. Green, *J. Chem. Phys.* **70**, 816 (1979), **70**, 4686 (1979).
- ⁴²A. E. de Pristo, S. D. Augustin, R. Ramaswamy, and H. Rabitz, *J. Chem. Phys.* **71**, 850 (1979).
- ⁴³S. Temkin, L. Bonamy, J. Bonamy, and D. Robert, *Phys. Rev. A* **47**, 1543 (1993).
- ⁴⁴L. Bonamy and F. Emond, *Phys. Rev. A* **51**, 1235 (1995).
- ⁴⁵X. Bruet, J. Bonamy, and M. L. Dubernet-Tuckey, *Chem. Phys.* (submitted).
- ⁴⁶J. Bonamy, D. Robert, and C. Boulet, *J. Quant. Spectrosc. Radiat. Transf.* **31**, 23 (1984).
- ⁴⁷C. Luo, R. Berman, A. Predoi-Cross, J. R. Drummond, and A. D. May, *J. Mol. Spectrosc.* **196**, 290 (1999).
- ⁴⁸E. W. Smith, M. Giraud, and J. Cooper, *J. Chem. Phys.* **65**, 1256 (1976).
- ⁴⁹C. Boulet and D. Robert, *Chem. Phys. Lett.* **60**, 162 (1978).
- ⁵⁰E. Rodrigues and J. M. Hartmann, *J. Quant. Spectrosc. Radiat. Transf.* **57**, 63 (1997). This reference emphasizes that the usual form of the sum rule ignores certain frequency factors. Such factors should be included in the analysis of the spectra and in testing the sum rule. We have estimated the effect of these factors in the present case and shown that they may safely be ignored in line mixing.
- ⁵¹Ph. Marteau, C. Boulet, and D. Robert, *J. Chem. Phys.* **80**, 3632 (1984).
- ⁵²J. Boisssoles, F. Thibault, C. Boulet, J. P. Bouanich, and J. M. Hartmann, *J. Mol. Spectrosc.* **198**, 257 (1999).
- ⁵³P. M. Sinclair, P. Duggan, R. Berman, A. D. May, and J. R. Drummond, *J. Mol. Spectrosc.* **181**, 41 (1997).